THE ASTROPHYSICAL JOURNAL, 370:L81–L84, 1991 April 1

HYDRODYNAMICAL INSTABILITIES AND MIXING IN SN 1987A: TWO-DIMENSIONAL SIMULATIONS OF THE FIRST 3 MONTHS

MARC HERANT AND WILLY BENZ
Harvard-Smithsonian Center for Astrophysics, 60 Garden Street, Cambridge, MA 02138
Received 1990 November 26; accepted 1991 January 8

ABSTRACT

We present results from numerical simulations of the early stages of the explosion of SN 1987A. Using a two-dimensional cylindrical geometry version of a smooth particle hydrodynamics code, we follow the explosion for 3 months to investigate both early hydrodynamical instabilities and the effect of the subsequent radioactive decay of ^{56}Ni and ^{56}Co with half-lives of 6.1 and 77.8 days, respectively.

We show that the mixing induced by hydrodynamical instabilities occurring during the first few hours is substantially modified at later time by the radioactive decay of ^{56}Ni and ^{56}Co. The inner cavity of the expanding supernova remnant fills up with nickel and its decay products thus forming a giant "nickel bubble." The peak velocity of the nickel increases by approximately 30% after the decays. While these results adequately model the core of the observed Fe line profiles, they fail to reproduce the high velocity wings of the spectra.

Subject headings: hydrodynamics — stars: supernovae

1. INTRODUCTION

SN 1987A has showed that mixing in the ejecta is part of the supernova explosion itself (Pinto & Woosley 1988). Observational evidence has pointed clearly in this direction: (1) the early detection of X-rays (Dotani et al. 1987; Sunyaev et al. 1987; Wilson et al. 1988) as well as of gamma-rays observed with the *SMM* satellite (Matz et al. 1988) and balloons (Mahoney et al. 1988; Sandie et al. 1988; Cook et al. 1988; Gehrels, Leventhal, & MacCallum 1988; Teegarden et al. 1989); (2) expansion velocities seen in line widths of infrared observations for various elements (Erickson et al. 1988; Witteborn et al. 1989) and in gamma-ray lines of ^{56}Co (Barthelmy et al. 1989); and (3) hydrogen velocities as low as 800 km s^{-1} found in the spectra 221 days after the explosion (Höflich 1988). Other, perhaps more indirect, indications came from the modeling of the optical light curve (Woosley 1988; Shigeyama, Nomoto, & Hashimoto 1988; Arnett & Fu 1989).

The existence of hydrodynamical instabilities behind the propagating shock had already been shown by Chevalier (1976) for suitable density distributions. Bandiera (1984) predicted that mixing should occur as a result of these instabilities. Using a realistic model for the supernova progenitor, Arnett, Fryxell, & Müller (1989, hereafter AFM89) and Fryxell, Arnett, & Müller (1991, hereafter FAM91) were able to show the impressive growth of convective fingers during the first few hours following the explosion in a number of two-dimensional numerical simulations. These simulations agreed with one-dimensional stability analyses (Ebisuzaki, Shigeyama, & Nomoto 1989; Benz & Thielemann 1990a) showing that the metal-helium and helium-hydrogen interfaces resulting from the evolution of the progenitor are the driving regions of the instabilities. In simulations with sufficient resolution, these authors found a double instability giving rise to "mushrooms inside mushrooms," the inner ones essentially made of metals and the outer ones essentially made of helium. FAM91 also derived velocity profiles of selected elements in order to compare with observations. They could show that oxygen, for example, was mixed up to close to 2000 km s^{-1} in velocity space whereas some hydrogen had a velocity as small as 300 km s^{-1} 3.6 hr after the explosion. Although these numbers seem to be fairly insensitive to the amplitude of the initial perturbations (for perturbations in velocity ranging from 5% to 20% peak-to-peak), FAM91 showed that the quantitative mass distribution of each chemical element as a function of velocity depends strongly on the perturbations applied to the initial conditions.

Hachisu et al. (1990, hereafter HMNS90) performed similar two-dimensional simulations. Besides the use of a different numerical approach (HMNS90 used a Lax-Wendroff scheme instead of a piecewise parabolic method) and the related question of resolution, both studies essentially differ in the internal structure of the supernova progenitor. FAM91's model has a smaller helium and metal core resulting in a steeper density gradient in the inner zones than in HMNS90's progenitor. As shown by Shigeyama et al. (1990) in one-dimensional linear stability analysis, smaller stellar masses result in more violent instabilities because of the steeper gradients in the inner regions. This is evidenced by the apparent absence in HMNS90 of the double-mushroom structure found by FAM91. After about 3000 s, HMNS90 obtain a single set of typical convective fingers engulfing both helium and the metals. The velocity distribution was found to have slightly higher peak velocities with some metals travelling at 2500 km s^{-1}. Some hydrogen is found with velocities slightly less than 1000 km s^{-1}. The same qualitative dependence on initial perturbations as in FAM91 is found in these simulations, too.

Although going a long way toward explaining the observations of SN 1987A, these results fall somewhat short of giving us the full picture. First and most important, the velocities obtained for the metals are smaller than the values derived from observations (see references above) implying velocities for ^{56}Co in the range of 2500–3500 km s^{-1}. Both groups pointed out that higher velocities might be obtained as a result of the energy released by radioactive decay of ^{56}Ni and ^{56}Co, whose potential importance for the hydrodynamical evolution of the remnant had already been mentioned by Woosley (1988) and

Arnett (1988). However, it was shown by Benz & Thielemann (1990b) that, if these elements are still located in the center of the exploding debris, the resulting instabilities and the associated clumping are insufficient to account for the observations. Work by FAM91 and HMNS90 has now clearly shown that at least some of the nickel becomes part of the finger-like structure a few hours after the explosion and that therefore the assumption of a spherically symmetric distribution of nickel is inadequate.

We present in this *Letter* results from simulations using a two-dimensional cylindrical geometry smooth particle hydrodynamics (SPH) code. Starting at $t = 300$ s after the initial explosion, we were able to run our simulations well past the nickel decay up to about 90 days, at which time we stop the calculations. We describe the initial conditions and the code very briefly in § 2 and the results in § 3. Finally, § 4 is devoted to the discussion of the results.

2. NUMERICAL METHOD AND INITIAL CONDITIONS

The two-dimensional cylindrical SPH code will not be described in detail here but is essentially the same as the three-dimensional SPH code described by Benz (1990). The code was tested against Sedov's blastwave solutions and shown to yield accurate results. We use a realistic equation of state including radiation pressure and a mean molecular weight determined locally from the detailed chemical composition. In all the simulations reported here, the overall conservation of total energy was found to be better than 0.1%. Nuclear energy release for the initially nickel particles is treated as a source term in the energy equation since we assume that the ejecta is optically thick.

To address the question of sensitivity to initial conditions, we have used both progenitors given by FAM91 and HMNS90. As in those two studies, a central explosion (10^{51} ergs) was initiated and the two progenitors were first evolved using a one-dimensional hydrodynamics code to $t = 300$ s. At that time, both one-dimensional models are transformed into a two-dimensional SPH representation assuming spherical symmetry. Unlike the situation with grid-based hydrodynamical codes, matching an arbitrary density structure to use as an initial condition for SPH is not a trivial problem since density is not a local quantity but is computed from weighted contributions of neighboring particles. We have developed an original mapping procedure which will be fully described in a forthcoming paper. In this instance, it reproduces the density distributions to within 5%, a small error compared to the other uncertainties associated with each model. This error is generally spherically symmetric and not random; it should therefore not contribute significantly to the seed perturbations introduced in the initial conditions. We have made use of the Lagrangian nature of SPH by increasing the number density of particles in regions of particular interest and, in addition, modeled only a 60° wedge centered on the equatorial plane. Periodic boundary conditions are applied on both sides of the wedge. Note that although it is only 60° wide, it can be shown from elementary geometry that such a wedge represents half the volume of the sphere; hence, it contains half the total mass of the star.

The instabilities are seeded by the introduction of random perturbations in velocity $\pm$ 10% in the material behind the shock. The length scale of these perturbations is determined by an overlying grid of 10 by 20 cells in the radial and polar directions, respectively. The physical origin of these perturbations (at least as far as their amplitude is concerned) is not completely clear; AFM89 and FAM91 suggest they originate from ^{16}O shell flashes when hit by the shock. Our results show similar dependence on the amplitude of the initial perturbations as found by FAM91 and HMNS90. We found that with perturbations of $\pm 5\%$ the results are nearly the same. The perturbations must be reduced to $\pm 1.25\%$ to observe a significant decrease in the amount of mixing. Reducing the length scale of the perturbations (20 by 40 grid) results generally in slightly less mixing, but the dominant wavelength of the instability remains identical and the same number of fingers grows.

3. RESULTS

For both progenitors, we have run simulations with particle numbers ranging from 3000 to 60,000. The variations in the principal features (size and number of fingers, amount of mixing, etc.) are minimal which enables us to determine that our resolution is sufficient to give us a converged solution of the problem (at least of the relevant aspects). To compare with the simulations of FAM91 and HMNS90, we show results at time $t = 400$ minutes. At this time, the instabilities related to the shock propagation are over and the effects of nickel and cobalt decay are still negligible.

As evident from Figure 1 (Plate L6 [*top*]) the progenitors lead to marked differences already after 400 minutes. The AFM progenitor results in two sets of mushrooms at the helium-metal interface and the hydrogen-helium interface, while the HMNS progenitor gives rise to a single set of mushrooms engulfing both interfaces. Another important difference is that the HMNS fingers reach further out than for the AFM model. This is translated into higher peak velocities for helium (2800 vs. 2100 km s^{-1}), the metals (2500 vs. 1800 km s^{-1}) and nickel (1100 vs. 900 km s^{-1}) for the HMNS case. In both cases some hydrogen is mixed inward down to approximately 500 km s^{-1}. All these results are in excellent agreement, both qualitatively and quantitatively with those published in FAM91 and HMNS90. Figure 2 shows the integrated line-of-sight velocity distribution for the metals and the nickel (a quantity directly comparable to observed line profiles in an optically thin medium) for the HMNS remnant. The line of sight was taken along the symmetry (z) axis. Note marked difference between the nickel and metal distribution. Since this feature would be preserved by a subsequent homologous expansion but is definitively not seen in observations the structure as computed at $t = 400$ minutes and homologously scaled to later times would *not* be a good match to observations of SN 1987A.

Assuming that the inner 0.075 $M_\odot$ of the original progenitors (allowing for a neutron star) consists of nickel, we carry the simulations further to 90 days after the explosion. As time goes by, nickel decays first into cobalt which decays in turn into iron resulting in a substantial amount of energy release (Woosley 1988). As the ejecta expand, the optical depth increases eventually leading to the escape of the energy. By 90 days, the energy deposition is certainly no longer local; hence, being spread over a larger amount of mass its effect becomes less and less important. In this respect our calculations represent an upper limit to the effect of nuclear energy input.

Figure 1 (*bottom*) shows the density and chemical structure of the envelope after 90 days for the HMNS90 progenitor. By this time the nickel, now essentially cobalt or iron, which was

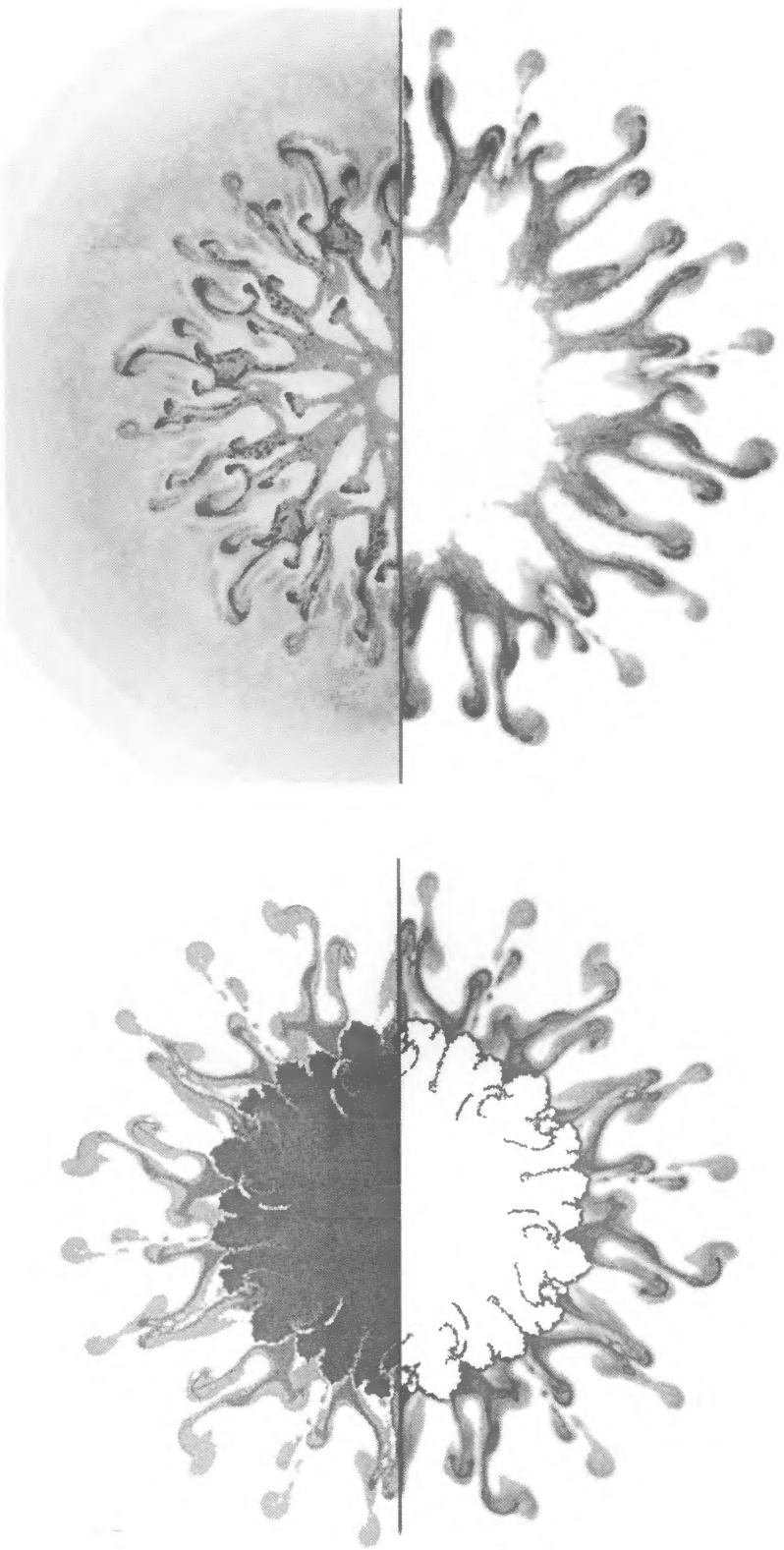

FIG. 1.—*Top:* Density structure of both progenitors (*right panel:* HMNS90; *left panel:* AFM89) at $t = 400$ minutes. Each panel consists of three 60° wedges added together. The average density contrast of the fingers is of order 2–3. *Bottom:* Density (*right panel*) and chemical composition (*left panel*) for the HMNS90 model at $t = 90$ days. In the left panel, H is white, He is light gray, metals are dark gray, and Co is black. Each panel was constructed by adding three 60° wedges together.

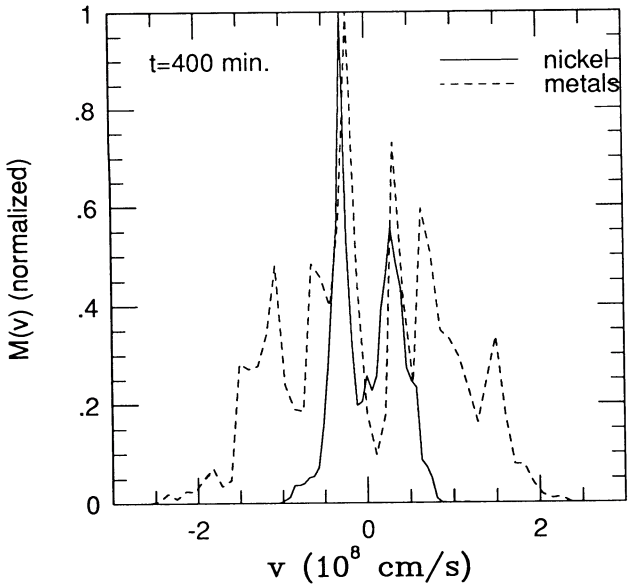

FIG. 2.—Integrated mass distribution as a function of projected line-of-sight velocity at $t = 400$ minutes for the HMNS90 model. Both curves have been normalized independently.

clumped in the fingers at $t = 400$ minutes has expanded to form a hot, low-density inner bubble. As it is heated by radioactive energy release, the nickel expands in all directions. Paths offering the least resistance are not directed outward along the fingers but rather inward and sideways. This results in the formation of a large, hot nickel bubble with pieces of crushed fingers forming high-density clumps of hydrogen, helium, and metals cut off from the rest of the outer ejecta. Later, the nickel also shows signs of creeping outward between the convective fingers. However, due to the relative low-density contrast of the fingers (factor of a few at most), this process is limited and the nickel never reaches extremely high velocities. It is possible that with increased resolution in the inner region, some small fraction of nickel could attain slightly higher velocities than found here.

Plotting again the integrated line of sight velocity distribution but now at time $t = 90$ days (Fig. 3) shows the dramatic effect of the nuclear energy release. Not only has the maximum velocity reached by the nickel increased substantially but the distribution has now a large core indicating that the nickel has indeed filled the inner cavity. It is worth noting that while this happens, the distribution of the other elements remains almost unchanged, except for a small increase of minimum velocities. In particular, we obtain small but significant amounts of hydrogen at velocities around 800 km s^{-1}, as is deduced from observations (Höflich 1988). Results obtained with the AFM progenitor are generally similar. The morphology of the nickel bubble is the same. The nickel progression to higher velocities is also similar, but the final peak velocity is commensurate to the lower nickel velocity at $t = 400$ minutes.

4. DISCUSSION

The main conclusion of our series of simulations is that nickel and subsequent cobalt decay does indeed boost the peak velocity of these elements significantly: 900 to 1300 km s^{-1} in the AFM model and 1400 to 1900 km s^{-1} in the HMNS model. Figure 3 can readily be identified with late-time iron line profiles; comparison with Fe II spectra from SN 1987A (Spyromilio et al. 1990) shows that we only slightly underestimate the half-width at half-maximum (HWHM) of the line (1000 vs. 1300 km s^{-1}) for the HMNS model. Higher velocities could be obtained by increasing the initial explosion energy (doubling the initial energy would result in a ~ 1.4 increase in velocity). However, the possible increase in velocity is limited to some extent by the observations of hydrogen at 800 km s^{-1} (Höflich 1988). The AFM model comes somewhat short of the HWHM in iron required by observations, whereas the HMNS model is marginally consistent. A more serious problem of the simulations is that the mass versus velocity distribution fails to reproduce the Fe II line wings which are observed to extend to ± 3500 km s^{-1}. The origin of this discrepancy has probably its roots in either major flaws in the progenitor models (which are still *very* uncertain), or in two-dimensional effects, or finally in a completely different mixing mechanism. We discuss briefly the last two points below.

One may rightfully question the validity of these results in three dimensions since two-dimensional cylindrical mushrooms are actually curly sheets in three dimensions, a highly unphysical outcome! In this context, it is interesting to note that the linear stability analysis of the problem yields the same results in two or three dimensions (for instance, growth rates obtained through a spherical harmonic expansion by Goodman 1990 and Ryu & Vishniac 1990 are independent of azimuthal wavenumber m). Therefore it is expected (and in fact confirmed from our preliminary three-dimensional calculations and those of Müller, Fryxell, & Arnett 1990) that the dominant wavelength of the instability ($\sim 15°$–$10°$ between mushrooms depending on how one counts them) will remain the same in three dimensions. However, it is unlikely that either the amount of mass mixed or the maximum velocities reached will be unchanged. It is probable that we overestimate the first (filling factor) and underestimate the second (Layzer 1955). Whether this will be sufficient to account for the high-velocity wings seen in the spectra remains to be seen, but it is

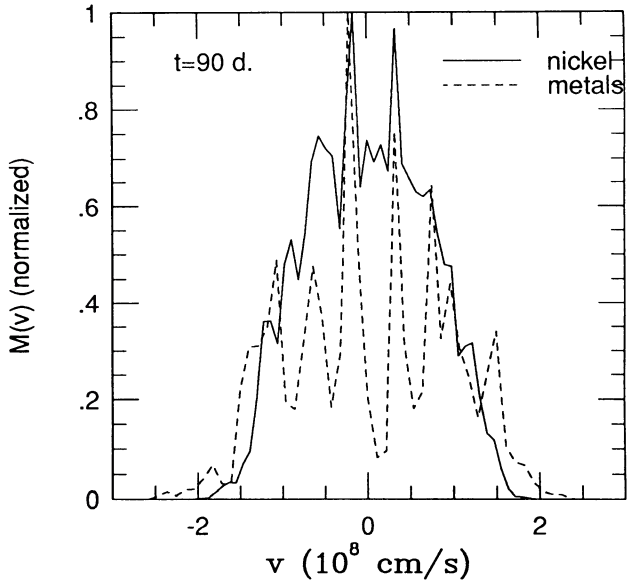

FIG. 3.—Integrated mass distribution as a function of projected line-of-sight velocity at $t = 90$ days for the HMNS90 model. Both curves have been normalized independently.

clear that a full understanding of the hydrodynamical instabilities in SN 1987A will require three-dimensional simulations, which is why we have restricted our present inquiries in two dimensions to a few simple cases. We reserve a thorough, forthcoming, study for the three-dimensional analysis. However, because of the limitations in three-dimensional resolution due to computer power, two-dimensional simulations will remain an essential guiding and testing tool in numerical investigations.

Finally, it is worthwhile noticing that the uncertainties in the explosion mechanism itself could allow for a completely different picture to emerge. Colgate (1990) has suggested that mixing will be obtained following instabilities at the interface of a high-entropy bubble formed around the neutron star and pushing on the ejecta. This would take place within the first 300 s leading to possibly a dramatically different outcome. Further investigations of this point will be necessary.

We would like to thank K. Nomoto, E. Müller, and D. Arnett for providing us with progenitor models as well as for many helpful discussions and comments during the preparation of this *Letter*. We would also like to thank F.-K. Thielemann, P. Pinto, and M. Davies for suggestions and enlightening discussions. Discussions with R. F. Stellingwerf regarding two-dimensional cylindrical geometry SPH are also gratefully acknowledged. This research was supported in part by NASA grant NGR 22-007-272. One of us (W. B.) also acknowledges partial support from the Swiss National Science Foundation.

REFERENCES

Arnett, W. D. 1988, ApJ, 331, 377
Arnett, W. D., & Fu, A. 1989, ApJ, 340, 396
Arnett, W. D., Fryxell, B., & Müller, E. 1989, ApJ, 341, L63 (AFM89)
Bandiera, R. 1984, A&A, 139, 368
Barthelmy, S., Gehrels, N., Leventhal, M., MacCallum, C. J., Teegarden, B. J., & Tueller, J. 1989, IAU Circ., No. 4764
Benz, W. 1990, in Numerical Modeling of Nonlinear Stellar Pulsation: Problems and Prospects, ed. J. R. Buchler (Dordrecht: Kluwer), p. 269
Benz, W., & Thielemann, F.-K. 1990a, ApJ, 348, L17
———. 1990b, in Supernovae, ed. S. E. Woosley (New York: Springer), p. 249
Chevalier, R. A. 1976, ApJ, 207, 872
Colgate, S. A. 1990, in Supernovae, ed. S. E. Woosley (New York: Springer), p. 352
Cook, W. R., et al. 1988, ApJ, 334, L87
Dotani, T., et al. 1987, Nature, 330, 230
Ebisuzaki, T., Shigeyama, T., & Nomoto, K. 1989, ApJ, 344, L65
Erickson, E. F., Haas, M. R., Colgan, S. W. J., Lord, S. D., Burton, M. J., Wolf, J., Hollenbach, D. J., & Werner, M. 1988, ApJ, 330, L39
Fryxell, B., Arnett, W. D., & Müller, E. 1991, ApJ, 367, 619 (FAM91)
Gehrels, N., Leventhal, M., & MacCallum, C. J. 1988, in Nuclear Spectroscopy of Astrophysical Sources (AIP Conf. Proc. 170) (New York: AIP), p. 87
Goodman, J. 1990, preprint
Hachisu, I., Matsuda, T., Nomoto, K., & Shigeyama, T. 1990, ApJ, 358, L57 (HMNS90)
Höflich, P. 1988, in IAU Colloquium 108, Atmospheric Diagnostics of Stellar Evolution, ed. K. Nomoto (Berlin: Springer), p. 288
Layzer, D. 1955, ApJ, 122, 1
Mahoney, W. A., et al. 1988, ApJ, 334, L81
Matz, S. M., Share, G. H., Leising, M. D., Chupp, E. L., Vestrand, W. T., Purcell, W. R., Strickman, M. S., & Reppin, C. 1988, Nature, 331, 416
Müller, E., Fryxell, B., & Arnett, W. D. 1991, in Proc. of ESO/EIPC Workshop on SN1987A and Other Supernovae, ed. J. Danziger, in press
Pinto, P. A., & Woosley, S. E. 1988, ApJ, 329, 820
Ryu, D., & Vishniac, E. 1990, preprint
Sandie, W. G., et al. 1988, ApJ, 334, L91
Shigeyama, T., Nomoto, K., & Hashimoto, M. 1988, A&A, 196, 141
Shigeyama, T., Nomoto, K., Tsujimoto, T., & Hashimoto, M. 1990, ApJ, 361, L23
Spyromilio, J., Meikle, W. P. S., & Allen, D. A. 1990, MNRAS, 242, 669
Sunyaev, R., et al. 1987, Nature, 330, 227
Teegarden, B. J., Barthelmy, S. D., Gehrels, N., Tueller, J., Leventhal, M., & MacCallum, C. J. 1989, Nature, 339, 122
Wilson, R. B., et al. 1988, in Nuclear Spectroscopy of Astrophysical Sources, ed. N. Gehrels & G. Share (New York: AIP), p. 66
Witteborn, F. C., Rank, D., Bregman, J. D., Pinto, P. A., Wooden, D., & Axelrod, T. S. 1989, ApJ, 338, L9
Woosley, S. E. 1988, ApJ, 330, 218